AGU PUBLICATIONS

JGR

Journal of Geophysical Research: Solid Earth

RESEARCH ARTICLE
10.1002/2017JB014037

Special Section:
Slow Slip Phenomena and Plate Boundary Processes

Insights into the causal relationship between slow slip and tectonic tremor in Guerrero, Mexico

Carlos Villafuerte[1] and Víctor M. Cruz-Atienza[1]

[1]Instituto de Geofísica, Universidad Nacional Autónoma de México, México City, Mexico

Key Points:
- The SSE slip rate modulates the TT and LFE occurrence rate in the whole tremor region of Guerrero
- The strength of the tremor asperities is 2.3 times smaller downdip in the sweet spot than updip in the transient zone
- The short-term SSEs take place right in the sweet spot, where tremor activity dominates during the interlong-term SSE period

Supporting Information:
- Supporting Information S1

Correspondence to:
C. Villafuerte,
villafuerte.cd@gmail.com

Citation:
Villafuerte, C., and V. M. Cruz-Atienza (2017), Insights into the causal relationship between slow slip and tectonic tremor in Guerrero, Mexico, *J. Geophys. Res. Solid Earth*, *122*, doi:10.1002/2017JB014037.

Received 26 JAN 2017
Accepted 6 AUG 2017
Accepted article online 11 AUG 2017

Abstract Similar to other subduction zones, tectonic tremors (TTs) and slow-slip events (SSEs) take place in the deep segment of the plate interface in Guerrero, Mexico. However, their spatial correlation in this region is not as clear as the episodic tremor and slip observed in Cascadia and Japan. In this study we provide insights into the causal relationship between TTs and SSEs in Guerrero by analyzing the evolution of the deformation fields induced by the long-term 2006 SSE together with new locations of TTs and low-frequency earthquakes (LFEs). Unlike previous studies we find that the SSE slip rate modulates the TT and LFE activity in the whole tremor region. This means that the causal relationship between the SSE and the TT activity directly depends on the stressing rate history of the tremor asperities that is modulated by the surrounding slip rate. We estimated that the frictional strength of the asperities producing tremor downdip in the sweet spot is around 3.2 kPa, which is ~2.3 times smaller than the corresponding value updip in the transient zone, partly explaining the overwhelming tremor activity of the sweet spot despite that the slow slip there is smaller. Based on the LFE occurrence-rate history during the interlong-term SSE period, we determined that the short-term SSEs in Guerrero take place further downdip (about 35 km) than previously estimated, with maximum slip of about 8 mm in the sweet spot. This new model features a continuum of slow slip extending across the entire tremor region of Guerrero.

1. Introduction

Recent advances in seismological and geodetic observatories have enabled recognizing a new class of slow tectonic phenomena occurring on the plate interface of different subduction zones worldwide [*Schwartz and Rokosky*, 2007; *Peng and Gomberg*, 2010]. Among these manifestations, slow-slip events (SSEs) release aseismically part of the strain accumulated on the transitional segments of the interface (updip and downdip of the seismogenic zone) and can last from days to several months [*Beroza and Ide*, 2011; *Obara*, 2011; *Schwartz and Rokosky*, 2007]. SSEs are very often accompanied by tectonic tremors (TTs) [*Obara*, 2002], which are sustained low-amplitude seismic signals more likely composed by the summation of low-frequency earthquakes (LFEs) produced by small shear dislocations near the plate interface [*Shelly et al*., 2007; *Ide et al*., 2007]. Each one of these seismic signals has a characteristic frequency content and represents an individual manifestation of a larger-scale tectonic release process [*Beroza and Ide*, 2011]. The clearest example of the spatiotemporal correlation between SSEs and TTs is the so-called episodic tremor and slip (ETS) observed in Nankai and Cascadia [*Rogers and Dragert*, 2003; *Obara and Hirose*, 2006]. Whereas in Cascadia and Nankai TTs occur within the zones of maximum slip rate of the SSEs (i.e., behind the slip front) [*Bartlow et al*., 2011; *Hirose and Obara*, 2010], in other subduction zones such as Bungo Channel in Japan, Hikurangi in New Zealand, and Guerrero in Mexico, TTs appear to be located apart in space supporting the idea that they are triggered by the increase of shear stress outside the slipping regions [*Hirose et al*., 2010; *Kostoglodov et al*., 2010; *Bartlow et al*., 2014].

We focus on the Guerrero subduction zone, Mexico, where long-term SSEs occur approximately every 3.5 years [*Cotte et al*., 2009; *Radiguet et al*., 2012] and represent the largest aseismic events in the world, with moment magnitude up to 7.6 [*Kostoglodov et al*., 2003, 2010]. In this region, the TT and LFE activity takes place in the horizontal segment of the plate interface beneath the continent [*Payero et al*., 2008; *Kostoglodov et al*., 2010], almost always concomitant with slow-slip transients [*Kostoglodov et al*., 2010; *Husker et al*., 2012; *Frank et al*., 2015b]. However, the spatial correlation between tremor and long-term SSEs is not as clear because the highest TT activity is shifted downdip about 50 km from the maximum slip of long-term SSEs (Figure 1a) [*Kostoglodov et al*., 2010; *Husker et al*., 2012].

Different studies of TTs and LFEs in Guerrero [*Payero et al*., 2008; *Kostoglodov et al*., 2010; *Husker et al*., 2012; *Cruz-Atienza et al*., 2015; *Frank et al*., 2014; *Maury et al*., 2016] show that these events concentrate in two main

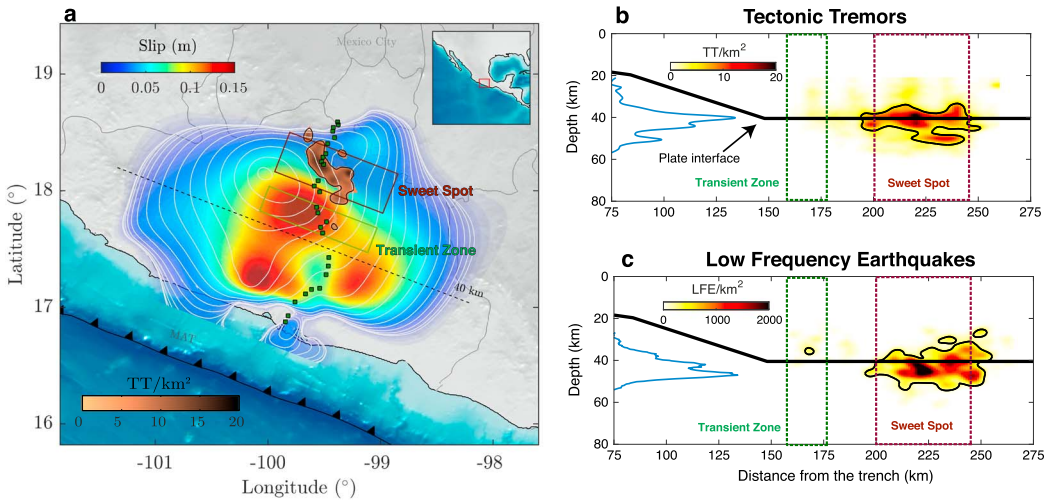

Figure 1. TT (this study) and LFE [*Frank et al.*, 2014] locations in Guerrero and slip distribution of the 2006 SSE [*Radiguet et al.*, 2011]. The green and maroon rectangles in the three panels indicate the transient zone and the sweet spot, respectively. (a) The blue-red colored region represents the cumulative slip of the 2006 SSE. The white contours show the rupture times for 2 cm cumulative slip every 20 days. The green squares indicate the location of the MASE array stations used to locate the TTs. The beige-black colors represent the cumulative TT density, and the black contour encloses the regions containing densities higher than 5 TT/km^2. The dashed line indicates where the plate interface becomes horizontal. (b and c) Cumulative TT and LFE densities projected onto a vertical trench-perpendicular section. The blue curves show normalized histograms for the TT and LFE hypocenters. Note that most of the tremor activity occurs between 40 and 45 km depth (i.e., at the plate interface and/or within the top 5 km of the oceanic crust).

source regions of the horizontal plate interface: the so-called sweet spot, downdip between 200–240 km from the trench, and the transient zone, located updip and close to the slab kink where it becomes horizontal, between 150 and 175 km from the trench (Figure 1) [*Husker et al.*, 2012; *Frank et al.*, 2014]. Unlike the transient zone, TTs and LFEs take place persistently in the sweet spot even in the absence of long-term events [*Kostoglodov et al.*, 2010; *Husker et al.*, 2012; *Frank et al.*, 2014]. For this reason, *Husker et al.* [2012] suggested that the sweet spot represents an interface segment with the optimal conditions of temperature, pressure, and fluid content to generate frequent tectonic tremor. In contrast, most of the tremor updip in the transient zone occurs during short episodes activated only during SSEs and, in some cases, during the passage of teleseismic waves [*Zigone et al.*, 2012].

During the interlong-term SSE periods there are TT and LFE episodes occurring approximately every 3 months in both the transient zone and the sweet spot [*Kostoglodov et al.*, 2010; *Husker et al.*, 2012; *Frank et al.*, 2015b]. This activity takes place simultaneously with very low amplitude displacements in the GPS records that have been associated with short-term SSEs [*Vergnolle et al.*, 2010]. The source inversion of these signals indicates that they are produced by moment magnitude ~6.4 SSEs located in the interface segment separating both tremor regions (i.e., the transient zone and the sweet spot) [*Frank et al.*, 2015b]. Current evidence of SSEs and tremor in Guerrero has thus led previous authors to propose different models to explain the activity of TTs in the sweet spot. *Kostoglodov et al.* [2010] suggested that given the spatial offset between the sweet spot and the 2006 SSE, the activity of TTs in the sweet spot is driven by the increase of shear stresses downdip of the SSE. Endorsing this argument, *Frank et al.* [2015a] concluded that variations in the LFE activity during the 2006 SSE were not associated with the slip rate at the interface, but rather with the increase of shear stresses in the sweet spot and the transient change of pore pressure close to the interface. In this study we report new high-resolution TT locations in Guerrero and analyze, along with a previously reported LFE catalog, their detailed spatiotemporal correlation with the strain field produced by the 2006 SSE to better elucidate both the causal relationship between slow-slip transients and tremor in the whole region and the actual location of short-term SSEs in Guerrero.

2. Tectonic Tremor Location in Guerrero

We relocated TTs in Guerrero by means of the tremor energy and polarization method (TREP) [*Cruz-Atienza et al.*, 2015] from broadband seismic data of the high-resolution Meso-American Subduction Experiment

(MASE, green squares in Figure 1a) [*Caltech*, 2007] recorded between the beginning of 2005 and mid-2007. During this period, a long-term SSE (~6 month duration) took place, providing us the opportunity to analyze the activity of TTs during the evolution of such a large aseismic transient. The tremor episodes were automatically detected using the spectral threshold method proposed by *Husker et al*. [2010] and correspond to those analyzed by *Husker et al*. [2012].

The TREP method determines TT hypocentral locations from the spatial distribution of the tremor energy, its spatial derivative, and the azimuth of the particle motion polarization ellipsoid. According to the source mechanisms reported for LFEs and VLFEs in the region [*Frank et al*., 2013; *Maury et al*., 2016], the method assumes horizontal fault planes and determines both the slip direction (i.e., the rake angle) and the source location that best explain the three above mentioned observables. This technique performs a grid search in a 3-D lattice with possible hypocenters beneath the study region. To do so, a synthetic Green's function database is precomputed for double-couple point dislocations. The Green's functions are calculated considering the 1-D layered velocity model proposed by *Campillo et al*. [1996] for the Guerrero province and the anelastic effects given by an attenuation relationship determined for the region [*García et al*., 2004]. The comparison between synthetic and observed data, as well as the uncertainty of the locations, is discussed in detail by *Cruz-Atienza et al*. [2015].

Unlike the TT locations reported by *Cruz-Atienza et al*. [2015] using the TREP method, for this work, we implemented a time-scan strategy along the entire tremor bursts using 1 min windows with 20 s overlap and considering theoretical moveouts for the *S* wave arrivals. We obtained 15,222 locations (Figure 1) with uncertainties smaller than 10 km assuming a grid increment of 5 km in the three Cartesian directions. This strategy allows us to analyze in detail the spatial variation of tremor sources during the observational period. Our final locations share features with those of previous studies, such as the concentration of TT sources downdip in the sweet spot and some activity with smaller density updip in the transient zone (Figure 1b). Depth of most tremors is well constrained around the plate interface at ~42 km and below, within the oceanic slab, up to a depth of 50 km as can be seen in the histogram on the left of Figure 1b. The comparison with the LFE locations by *Frank et al*. [2014] is remarkable in both the trench-perpendicular and vertical directions (compare Figures 1b and 1c), supporting the idea that tremor is composed of LFE swarms [*Shelly et al*., 2007]. In contrast with the LFE catalog [*Frank et al*., 2014], our tremor locations using the TREP method have good resolution in the along-strike direction (i.e., in the array-perpendicular axis). As shown by *Cruz-Atienza et al*. [2015], resolution lengths in that direction are similar to those in the trench-perpendicular direction. This allows us to analyze the occurrence of TTs along dip and along strike over the horizontal plate interface during the propagation of the SSE.

Figure 1a shows both our TT locations and the final slip distribution of the 2006 SSE determined by *Radiguet et al*. [2011]. The slip propagation of this event does not exhibit a simple unilateral trend (see rupture times with white contours). It nucleates at the downdip portion of the interface and simultaneously spreads updip and bilaterally in the trench-parallel direction. The sweet spot (maroon rectangle) is located in the downdip limit of the maximum slip, as previously discussed by *Kostoglodov et al*. [2010]. Although the maxima of slip are updip and do not coincide with the sweet spot, there is a small amount of slip (around 5 cm) that accommodates in the main TT source area (i.e., in the sweet spot). It could be argued though that such small slip may be an artifact due to the smoothing procedure involved in the source inversion. However, since the sweet spot lies in a region with highest confidence for the inverted slip according to the resolution matrix reported by *Radiguet et al*. [2011], the slip mapped there is very likely to be real.

3. Elastic Fields Induced by the 2006 SSE

To investigate the causal relationship between the 2006 SSE and the associated TTs in Guerrero, following *Rivet et al*. [2011, 2013], we used a three-dimensional (3-D) finite difference code for solving the velocity-stress formulation of elastodynamic equations [*Olsen et al*., 2009] to track the quasi-static evolution of the stress field induced by the slow-slip history inverted by *Radiguet et al*. [2011] considering 20 day time steps. Our velocity model, which is the same used by *Rivet et al*. [2011], integrates a trench-perpendicular tomographic structure [*Iglesias et al*., 2010] extended in the trench-parallel direction and takes into account the geometry of the plate interface and the elastic properties of the upper oceanic crust inferred by previous studies [*Pérez-Campos et al*., 2008; *Kim et al*., 2010]. Details of the 3-D velocity structure can be found in *Villafuerte* [2016].

Using this numerical model we obtained the stress tensor and the volumetric changes (i.e., the trace of the stress tensor) at every point of our 3-D domain associated with every slip increment of the SSE. We thus solved for the normal and shear stresses acting on fault planes parallel to the plate interface that we have assumed horizontal in the tremor region according to its geometry [*Pérez-Campos et al*., 2008] and recent observations of TTs [*Cruz-Atienza et al*., 2015], LFEs [*Frank et al*., 2013], and very low frequency earthquakes (VLFEs) [*Maury et al*., 2016] in Guerrero, which have focal mechanisms with zero or very low dipping angles. We then estimated pore pressure changes from the volumetric strain field assuming undrained conditions as

$$\Delta p = -B\frac{\Delta\sigma_{kk}}{3}, \tag{1}$$

where $\Delta\sigma_{kk}$ is the change of dilatancy and B represents the Skempton coefficient ranging from 0 to 1, where the rock is fluid-saturated for B close to 1. This relation implies that changes of dilatancy every 20 days are instantaneously translated into changes of pore pressure. Since the permeability is low within the oceanic crust [*Audet et al*., 2009; *Peacock et al*., 2011; *Perry et al*., 2016] where fluids are likely to be present in Guerrero [*Song et al*., 2009; *Kim et al*., 2010], fluid diffusion is slow enough to make our approach valid for the time span of the SSE [*Villafuerte*, 2016]. To confine fluids within the top 5 km of the subducted slab we considered $B = 0.9$ in that layer and $B = 0$ elsewhere.

To quantify the combined effect of the normal and shear stresses along with the pore pressure, we computed the Coulomb failure stresses (CFSs). Assuming a fault friction coefficient, μ, the CFS indicates how prone is a rock to failure on a specific fault orientation following the relation:

$$\Delta\mathrm{CFS} = \Delta\tau + \mu(\Delta\sigma_N + \Delta p), \tag{2}$$

where $\Delta\tau$ represents the change of shear stress on the fault plane in the slip direction, $\Delta\sigma_N$ is the change of the fault normal stress (positive for tension), and Δp is the change of pore pressure that counteracts the effect of $\Delta\sigma_N$. Since $\Delta\tau$ induced by the SSE is almost an order of magnitude larger than the corresponding values for $\Delta\sigma_N$ and Δp, the CFSs do not significantly change for different friction coefficients. We have though assumed a friction coefficient of 0.2, which is in general agreement with recent estimates in regions where slow phenomena occur [e.g., *Thomas et al*., 2009, 2012; *Houston*, 2015].

4. Spatiotemporal Correlation Between TTs and the 2006 SSE

Figures 1b and 1c show that TTs and LFEs are remarkably well confined to depths close to the plate interface. Since we are interested in the along-dip and along-strike variations of tremor activity and how they are correlated with the elastic fields induced by the SSE near by the interface, for the analysis, we only considered TT locations between 40 and 50 km depth (i.e., at the interface and within the subducted slab), the slip on the plate interface, and the ΔCFS over a horizontal plane 2 km below the plate interface. Figure 2 shows the evolution of both the 2006 SSE and the associated CFS, along with the occurrence of TTs in the corresponding time windows. CFS (right column) is only shown where it is numerically well resolved by our finite difference method (i.e., in the volume containing the horizontal segment of the plate interface). We notice that ΔCFS at parallel planes within the first 5 km below the plate interface are essentially the same, so the solution at the chosen depth is representative of the deformations taking place within the upper oceanic crust. When estimating the pore pressure we assumed that fluids are uniformly distributed along the slab, which may be not necessarily true considering possible dehydration pulses in specific slab segments as inferred from mineralogical phase transformations and thermal modeling [*Manea and Manea*, 2011]. However, given the large uncertainties in the fluid content, for the sake of simplicity and to identify first-order correlations with the TT activity, we kept our hypothesis in the analysis.

In order to identify the parameter that actually triggers tremor in the whole SSE region, as a first approach, we analyzed the spatiotemporal consistency of tremor activity with (1) slipping regions of the plate interface and (2) with interface region where ΔCFS is positive. To do so, for each 20 day window of the SSE, we quantified the percentage of TTs in each window occurring over regions with slip increments larger than 5 mm and ΔCFS higher than 5 kPa. Figure 3 summarizes the results of this exercise, where we find that there is a much higher spatiotemporal consistency of TT activity with slip (red bars) than with ΔCFS (blue

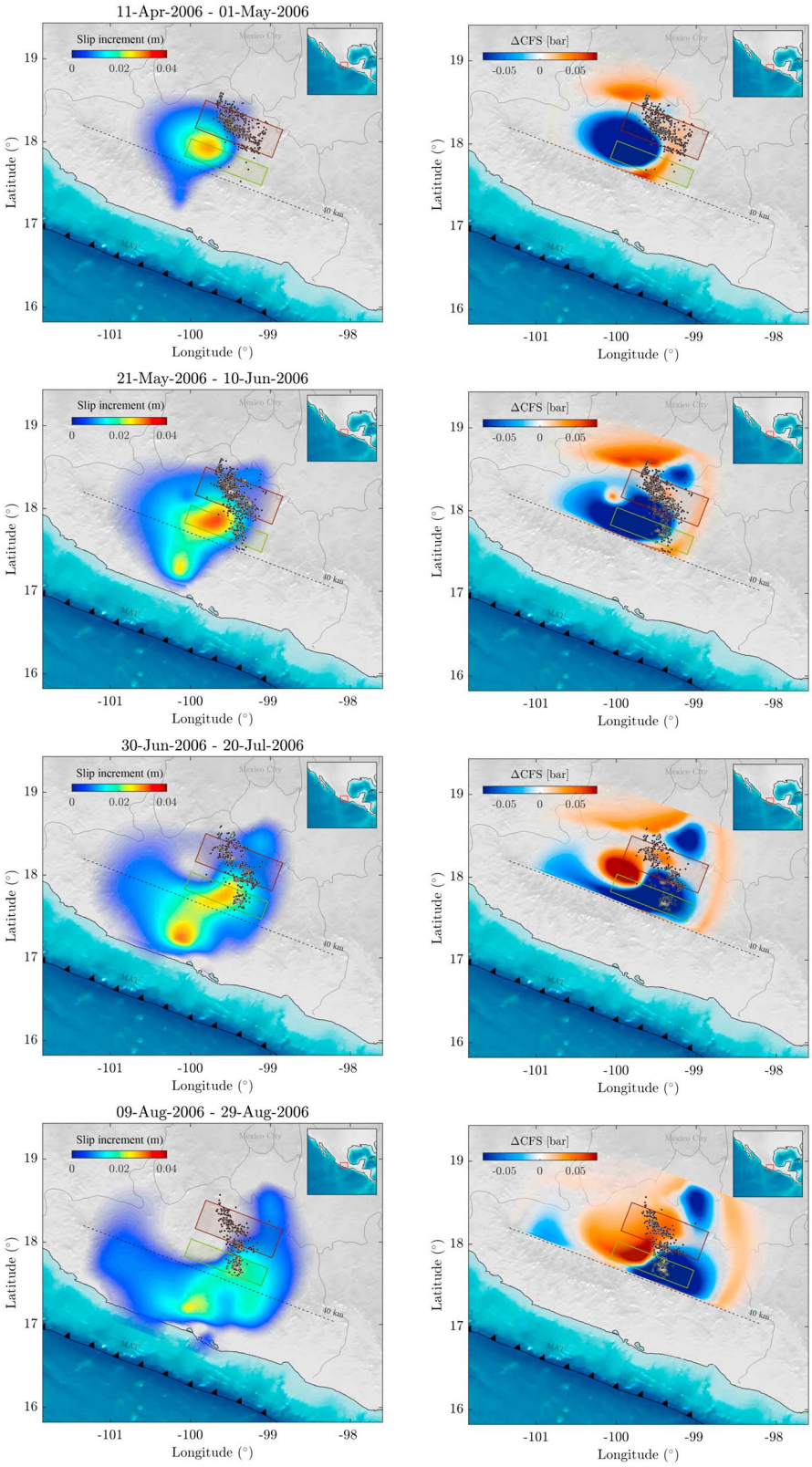

Figure 2. Snapshots of the slip increment for the (left column) 2006 SSE and the (right column) associated ΔCFS computed over a horizontal plane 2 km below the plate interface. The black dots indicate the associated TTs occurring during the corresponding time window. The green and maroon rectangles represent the transient zone and the sweet spot, respectively. The dashed line indicates where the plate interface becomes subhorizontal.

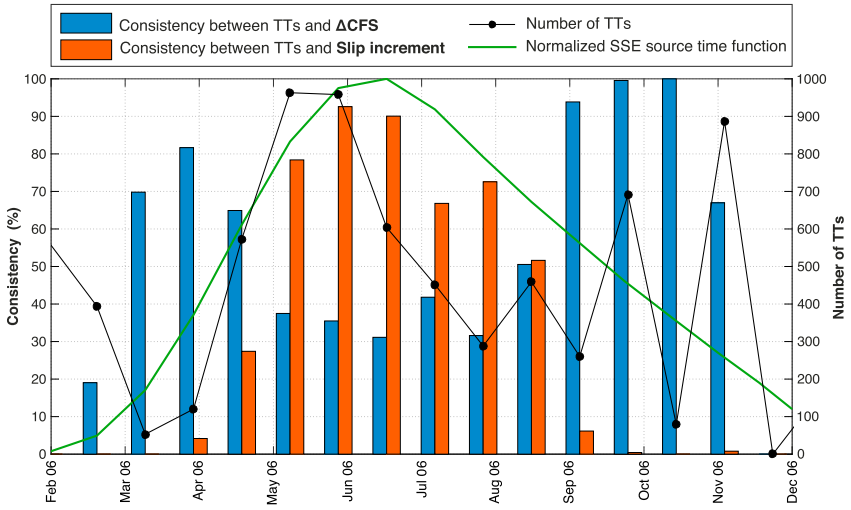

Figure 3. Consistency between the TT occurrence and the 2006 SSE-induced elastic fields. The bars represent the percentage of TTs in each time window located within regions with values of ΔCFS larger than 5 kPa (blue bars) and within regions with slip increments larger than 5 mm (red bars) for every 20 day slip increment of the 2006 SSE (left axis). The black line shows the number of TTs associated with each window (right axis). The green line shows the normalized source time function (STF) of the SSE along the horizontal segment of the plate interface.

bars) during the most intense phase of the SSE (i.e., between May and August, where the green line depicts the SSE source time function, STF). The trend is different at the beginning and the end of the SSE, where the STF starts growing and falls to zero, respectively. At those stages, TT activity is more consistent with increments of CFS.

Histograms in Figure 3 essentially give us an integrated idea of the temporal correlation between the SSE-induced elastic fields and tremor activity in the whole region. Thus, to generate detailed maps showing their spatiotemporal correlation, we divided our horizontal domain into bins of 3×3 km. In each bin we extracted the time series of the SSE-induced fields (i.e., the slip rate and ΔCFS time series) and the TT counts during the whole duration of the SSE. Figure 4 shows some examples of those series in three representative bins with locations shown in Figure 5 (small squares). Whereas there is no visual correlation between the TT activity and the evolution of ΔCFS (upper panels) at these bins, the correlation between the TT activity and the slip rate is remarkable (lower panels). To quantify the similarity of the time series in the whole region, for each bin, we computed the correlation coefficient (CC) between the TT time series and those associated with both SSE-induced fields. Values of CCs for the series of Figure 4 are reported inside each panel, where positive high values are only found for the slip rate time series (lower panels).

Figure 5 presents the resulting spatial distributions of CCs in the study region. These maps allow delineating the regions where there is (or there is not) a significant spatiotemporal correlation between the TT activity and the evolution of both the SSE slip rate (top panel) and the associated ΔCFS (bottom panel). As previously shown in Figure 4, the evolution of ΔCFS has very low, if any, positive correlation with the activity of TTs during the SSE in the entire study region. In contrast, the slip rate correlates very well with the tremor activity in both the transient zone and the sweet spot, the latter being a region where previous studies found difficult to conciliate the tremor rate with the slip evolution of the SSE [e.g., *Kostoglodov et al.*, 2010; *Frank et al.*, 2015a]. To quantify the statistical significance of the estimated CCs, we performed a goodness-of-fit test under the null hypothesis that the slip rate and the occurrence of TTs are not temporally correlated. Figure S1b in the supporting information shows that regions where we found high CCs values present low *P*-values ($p < 0.05$), implying that our correlation estimates there provide a significant result and that the null hypothesis can be rejected at the 95% confidence level.

In addition, we calculated the CC between the evolution of the pore pressure and the occurrence of TTs and found a good correlation in the sweet spot (Figure S2, left panel). However, the occurrence of TTs and the evolution of the normal stress are highly anticorrelated in the same region (Figure S2, right panel), which implies that both fields, the pore pressure and the normal stress, counteract each other, making it difficult to associate

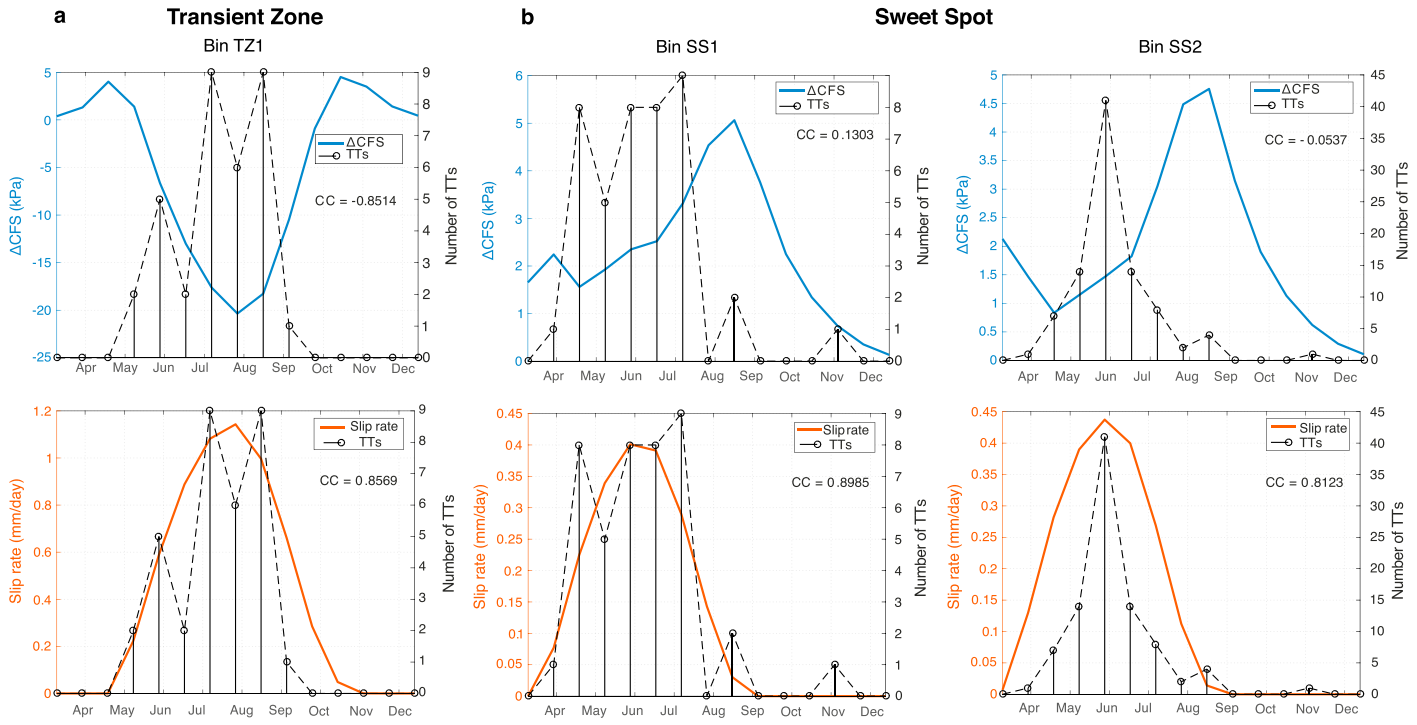

Figure 4. Comparison between the activity of TTs and the evolution of the SSE-induced fields in three representative spots of the plate interface (columns). Correlation coefficients (CCs) between the TTs time series (black) and the evolution of the ΔCFS (blue) and the slip rate (red) are shown inside each panel. The 3 × 3 km spots are located in the transient zone (a) and the sweet spot (b), as shown in Figure 5a.

the evolution of pore pressure with variations in the activity of TTs. We can only conclude then that pore pressure inhibits the clamping effect of the normal stress to maintain very low effective stresses in the sweet spot.

5. Correlation Between LFEs and SSEs

We now compare the evolution of the SSE-induced fields with the long-term activity of LFEs. The large amount of events detected and located almost continuously by *Frank et al.* [2014] brings us the opportunity to do such comparison not only during the 2006 SSE but also during the preceding inter-SSE period, where short-term SSEs have been identified [*Vergnolle et al.*, 2010; *Frank et al.*, 2015b].

Following *Frank et al.* [2015a], we first obtained the LFE rate from their cumulative count in different segments of the plate interface with increasing distance from the trench (Figure S3a). To make an appropriate comparison with the SSE-induced fields that have a time resolution of 20 days, we filtered the LFE occurrence-rate time series in every segment for periods longer than 40 days (Figures S3b and S3c). The black curves of Figure 6 show the averages of the time series along both the transient zone (left) and the sweet spot (right). As previously noticed by *Frank et al.* [2015a], two main features arise from the analysis: (1) the LFE rates in both the transient zone and the sweet spot largely increase during the 2006 long-term SSE, and (2) there exist isolated peaks of LFE activity in both regions during the inter-SSE period associated with short-term SSEs [*Frank et al.*, 2015b]. Figure 6 also shows that the rate of LFEs in the sweet spot during the short-term SSEs is as high as the maximum rate observed during the 2006 long-term SSE. This last feature is not present in the transient zone, where bursts of LFEs during the short-term SSEs are only one fifth of the maximum rate observed during the 2006 SSE. To compare the rate of LFEs with the SSE-induced fields, we subtracted from the time series (Figures S3b and S3c) the secular seismicity rate in each region (i.e., the minimum value of the time series) to preserve only the changes of activity associated with the short- and long-term SSEs. We then computed, for every 20 day increment, the average of the 2006 SSE-induced fields along the transient zone and the sweet spot (i.e., the average of each field inside the

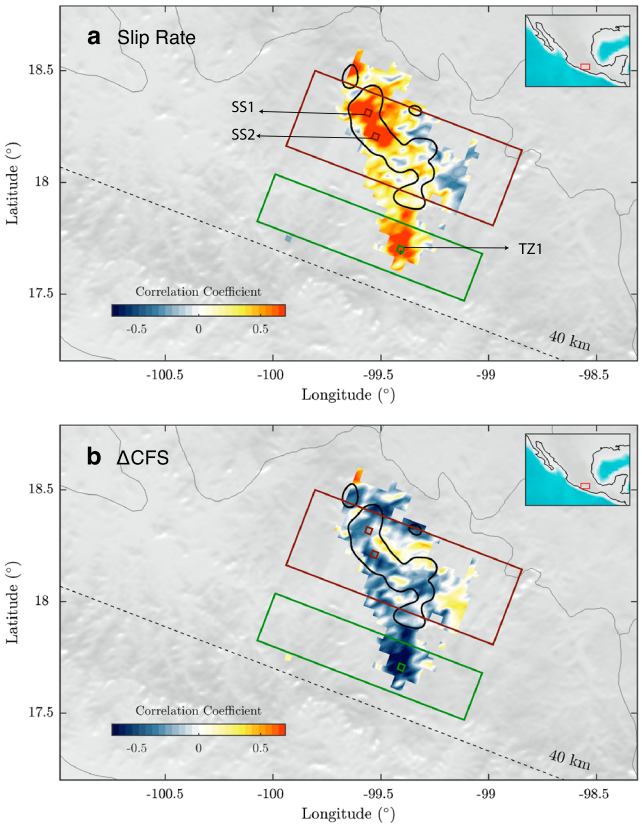

Figure 5. Correlation coefficients between the activity of TTs and the evolution of the (a) slip rate and the (b) ΔCFS during the 2006 SSE. The black contours indicate the regions with the highest occurrence of TTs. The squares indicate the 3 × 3 km bins where the time series shown in Figure 4 were extracted for the TT and SSE-induced fields. The green and maroon boxes indicate the transient zone and the sweet spot, respectively.

rectangles shown in Figure 5). Tests for different geometries and sizes for the rectangular regions gave essentially the same results.

To make possible the comparison of the LFE time series with the evolution of the SSE-induced fields including the interlong-term SSE period, we approximated the slip distribution of the short-term SSEs found by *Frank et al.* [2015b] with a two-dimensional (2-D) Gaussian function by taking care of fitting the best possible each slip contour (please notice in Figure S4 how close is our approximation for values larger than 2 mm to the slip distribution reported in Figure 1a of *Frank et al.* [2015b]). To validate the elliptical slip approximation, which neglects some small values (<2 mm) close to the shore and down-dip, we compared the associated surface displacements (computed with our 3-D finite difference model) with the corresponding GPS measurements reported by *Frank et al.* [2015b] (Figure S4). Although our displacement predictions slightly differ from those of *Frank et al.* [2015b], they explain fairly well the observations, especially in the closest three stations where displacements are larger than 1 mm, and the data errors are smaller than the actual displacements. Given the small duration of the short-term events, we assumed a 7 day width (Gaussian) slip rate function that corresponds to the maximum duration of the LFE bursts reported by *Frank et al.* [2014] in the same period. The times for the maxima of the slip rate functions were chosen to coincide with the times of the maxima of the LFE rate history during the interlong-term SSE period. This procedure allows us to quantify also the average of the elastic fields induced by the short-term SSEs reported by *Frank et al.* [2015b] in both

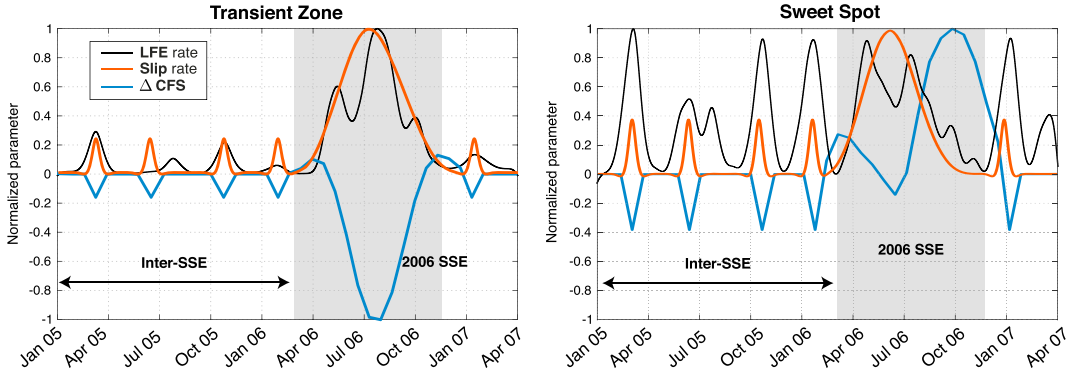

Figure 6. Comparison between the evolution of the SSE-induced fields and the occurrence rate of LFEs (black lines) in the (left) transient zone and the (right) sweet spot. The evolution of the ΔCFS and the slip rate is represented by the blue and red curves, respectively, during the 2006 SSE (shaded area) and the inter-SSE period.

the transient zone and the sweet spot (rectangles of Figure 5) in the same way we did for the 2006 long-term SSE (i.e., by solving the 3-D elastodynamic equations for the slow-slip distribution).

Figure 6 shows the resulting comparison, where ΔCFS (blue curves) does not correlate (positively) with the LFE rate (black curves) neither in the sweet spot nor the transient zone. During the 2006 long-term SSE, ΔCFS is anticorrelated with the activity of LFEs in the transient zone, and its maximum in the sweet spot is delayed more than 2 months from the corresponding LFE rate maximum. In contrast, the slip rate in both regions during the long-term SSE is well correlated with the occurrence rate of LFEs. These results are consistent with our findings of section 4 regarding the TT activity, where we concluded that tremor is better correlated in space and time with the long-term SSE slip rate than with the associated ΔCFS.

During the interlong-term SSE period (i.e., outside the shaded areas of Figure 6), while the slip rate (red curves) amplitudes in the transient zone (left panel) follow pretty well the observed rates of LFEs associated with the short-term SSEs, in the sweet spot (right panel), they are much smaller (more than 60%) than expected (compare black and red curves). One possible reason for this discrepancy is that the short-term slip distribution inverted by *Frank et al*. [2015b] is located in the wrong place. We notice that given the extremely small GPS amplitudes associated with these events, *Frank et al*. [2015b] had to stack GPS time series from different short-term SSEs getting uncertainties much larger than most of their observations (see Figure S4). They found, however, that the short-term slip patches are located south (i.e., trenchward) of the sweet spot (see Figures 7a and S4).

6. Finding the Actual Location of the Short-Term SSEs

Our results of sections 4 and 5 show that the slip rate on the plate interface is the parameter that better correlates with tremor activity during the most active phase of the long-term 2006 SSE in both the transient zone and the sweet spot. It is thus reasonable to think that the slip rate modulates the LFE rate, as suggested by *Frank et al*. [2015b] when interpreting LFE activity in terms of deep slip transients in the same region. We then should expect the slip rate function to mimic the tremor (and LFEs) rate evolution during the short-term SSEs in the same way we have shown to be the case during the long-term 2006 event. By using this expectation as an observational constraint, we can infer the slip distribution of the short-term SSEs that best explain the rate of LFEs in both source regions.

The slip rate functions shown in Figure 6 during the interlong-term SSE period (red curves outside the shaded areas) were computed from our elliptical approximation of the short-term slip distribution proposed by *Frank et al*. [2015b] (Figure S4). The fit with the LFE rate (black curves) is far from satisfactory in the sweet spot. We then performed a grid search to look for the size and position of the elliptical slip patch, both in the along-dip direction, that best explain the LFE rate in the two tremor regions (i.e., in the sweet spot and the transient zone). We define the size of the slip patch along both ellipse axes as the distance between the slip contours limiting 0.99 cumulative probability of the Gaussian distributions, which correspond approximately to the distance separating the slip contours with 5% of the maximum slip. The patch size in the along-strike direction was fixed to 130 km because this value minimizes the error function defined below to evaluate the goodness of the slip models. The grid search then explored slip patches with different along-dip dimensions and positions, so that all patches have the same moment magnitude equal to 6.4, reported as the upper limit for the short-term SSEs by *Frank et al*. [2015b]. Since the slip distributions are given by 2-D Gaussian functions, to match the chosen magnitude, the method automatically adapts the maximum slip values at the center of the ellipses.

The most prominent difference between the transient zone and the sweet spot is the relative amplitudes of the LFE rate functions (black curves in Figure 6) during the short- and long-term SSEs. While the amplitude ratio in the sweet spot between most short-term SSEs and the long-term SSE is nearly one, in the transient zone, the average ratio is about five. We thus define the goodness of a given slip model as the average error of the slip-rate amplitude ratio in both tremor regions. If the observed LFE ratio is defined as r_o and the predicted slip-rate ratio as r_p, the model error in each region is then given by $(r_o - r_p)/r_o$. Figure 7b shows the goodness of all slip models explored in the grid search. Although the resolution for the slip patch location is better (vertical axis) than the patch size (horizontal axis), the optimal slip model is clearly located 215 km away from the trench (i.e., right in the sweet spot and thus ~35 km farther downdip from the position determined by *Frank et al*. [2015b]) and has 170 km length (white start) with maximum slip of 8.0 mm.

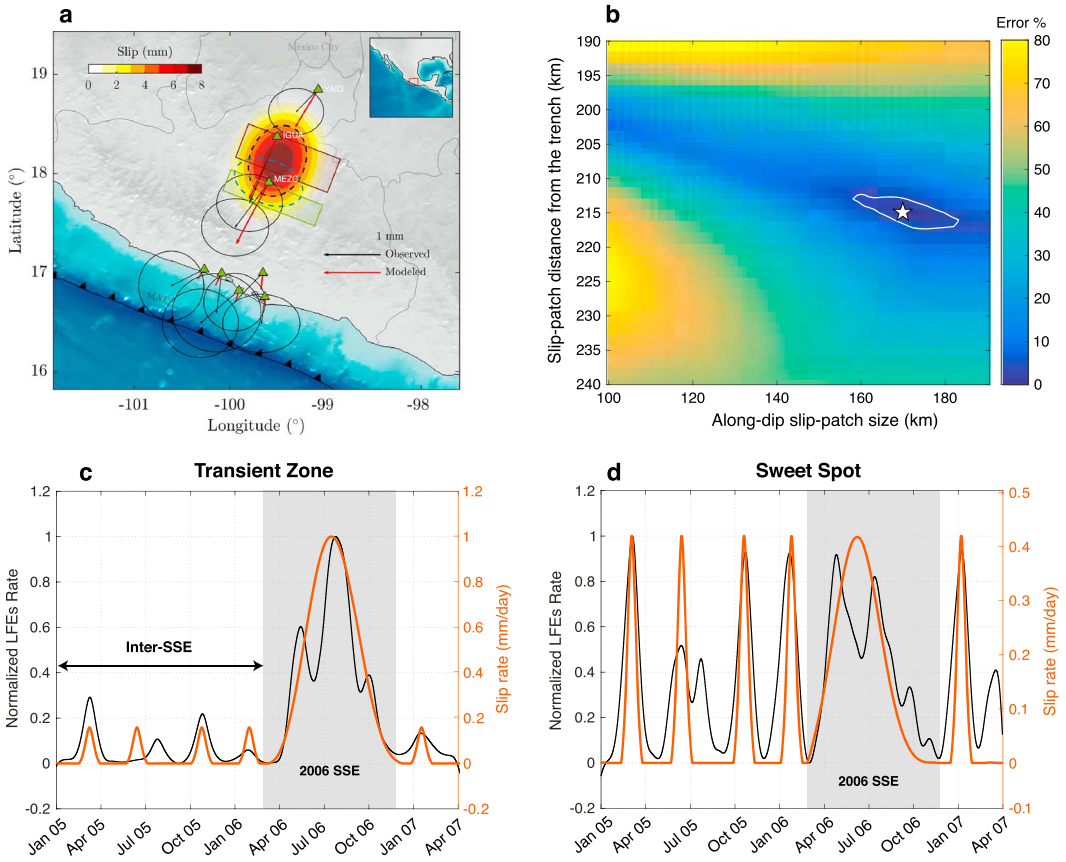

Figure 7. Location of the short-term SSEs and evolution of the slip rate in the tremor regions. (a) Slip distribution (color map) determined for the short-term SSEs that best explains the LFEs occurring rate in both transient zone and sweet spot during the inter-SSE period. The dashed blue ellipse approximates the 4 mm isoslip contour of the short-term SSE found by *Frank et al.* [2015b] (see Figure S4). The black dashed ellipse delineates the same isoslip contour for our model. The green triangles represent the local GPS stations and the black arrows the observed GPS displacement vectors with their respective error ellipses. The red vectors correspond to the displacement predicted by our slip distribution obtained from the grid search. The green and maroon rectangles represent the transient zone and the sweet spot, respectively. (b) Cost function for the slip models explored in the grid search. The white star indicates the slip model that presents the best fit, and the white contour encloses the models with errors smaller than 5%. (c and d) The fits between the slip rate (red curve) and the LFE rate (black curve) in the transient zone and the sweet spot, respectively, including our preferred short-term slip model.

The optimal slip model is shown in Figure 7a, where we also compare the observed GPS displacements determined by *Frank et al.* [2015b] for the short-term SSEs with the displacements predicted by the model. Considering the very large GPS data uncertainties (circles in Figure 7a), we did not use the GPS displacements to resolve the inversion because many different slip distributions may formally explain the geodetic observations in the same way, providing no useful information. In this sense, our displacement predictions are as good as those reported by *Frank et al.* [2015b] for their slip distribution. The difference between both models is that our slip distribution also explains the LFE rates in both tremor regions. This can be seen in Figures 7c and 7d where we show that, unlike *Frank et al.*'s model (red curves in Figure 6), the slip-rate functions predicted by our slip distribution satisfy the expected behavior in both tremor regions (i.e., the relative slip-rate amplitudes during both short- and long-term SSEs) when compared with the rate of LFEs (black lines).

The along-dip extension of our slip model indicates that the short-term SSEs are likely to take place mainly in the sweet spot, although they also reach the transient zone. In the transient zone (i.e., at ~170 km from the trench), a slip larger than 2 mm is required for the slip rate to match the observational condition imposed by the LFE rate. Figure 8 shows an overview of the SSEs in Guerrero (blue and red curves) along with our tectonic tremor locations (color shades) and LFEs (gray curves). Unlike previously suggested, we can see that most of

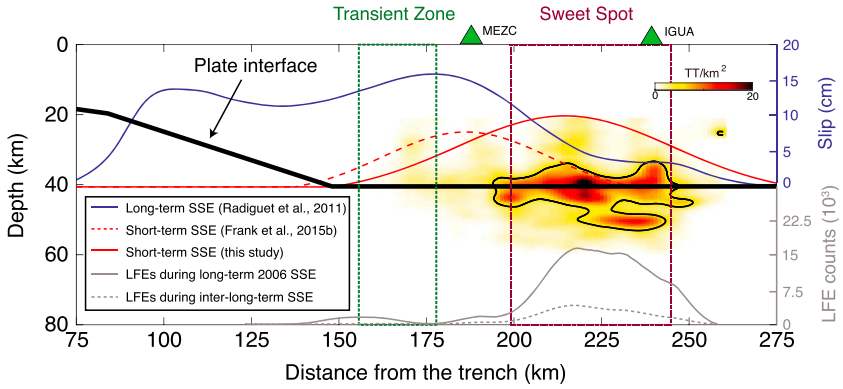

Figure 8. Overview of the slow earthquake activity in Guerrero. Final slip distribution for the 2006 SSE (blue curve) below the MASE array [*Radiguet et al.*, 2011]. Slip distributions for the short-term SSEs determined in this study (red curve) and by *Frank et al.* [2015b] (red dashed curve) are multiplied by a factor of 12 for comparison purposes with the long-term 2006 slip distribution. The thick black line sketches the geometry of the plate interface. The green and maroon dashed boxes indicate the location of the transient zone and the sweet spot. The green triangles represent the local GPS stations. The density of TTs shown in color shades (this study) is the same as in the Figure 1b, and the gray curves show the LFE histograms during both the long-term 2006 SSE (solid) and the interlong-term SSE periods (dashed).

the TT and LFE activity taking place in the sweet spot coincides with the plate interface segment where the short-term SSEs occur according with our analysis.

7. Discussion

The comparison of the SSE-induced fields with independent observations of TTs and LFEs in Guerrero suggests that the SSE slip rate in the plate interface is the parameter that controls the occurrence rate of these seismic events in the whole tremor region (i.e., updip in the transient zone and downdip in the sweet spot). During the long-term 2006 SSE, the rate of LFE sources is similar in both regions [*Frank et al.*, 2015a]. However, the maximum slip rate in the sweet spot is approximately half of the maximum value observed in the transient zone (see Figures 7c and 7d). This implies that there is a significant difference between both regions in terms of frictional properties that could be interpreted as variations of the tremor asperities' yielding strength. To estimate the strength level of the tremor asperities, we calculated the peak to residual stress drop associated with the maximum slip rate in the two tremor regions. To do so we considered a simple relationship for antiplane shear cracks stating that the ratio of the slip-front propagation speed, V_{prop}, and the slip rate, V_{slip}, can be approximated as the ratio of the elastic shear modulus, G, and the peak-to-residual stress drop, $\Delta\tau$, in the slipping front as [*Ida*, 1973; *Shibazaki and Shimamoto*, 2007; *Rubin*, 2011; *Rubin and Armbruster*, 2013]

$$\frac{V_{\text{slip}}}{V_{\text{prop}}} = \frac{1}{a}\frac{\Delta\tau}{G}, \tag{3}$$

where α is a geometric constant that depends on the spatial distribution of the stress drop behind the slip front. For slow dislocations such as shown in Figure 2 or those observed in Cascadia during the ETS, the length of the slip front, W, is much larger than the distance between the front and the place where the slip has reached its final value, L (i.e., $W \gg L$). In these cases, $\alpha = 1/\pi$ is the more appropriate choice for a uniform stress drop distribution [*Rubin and Ampuero*, 2009; *Hawthorne et al.*, 2016]. Assuming a shear modulus of 18 GPa [*Royer et al.*, 2015] and a constant SSE propagation speed of 0.8 km/d [*Radiguet et al.*, 2011], by taking the average of the maximum slip rates as 1 and 0.45 mm/d for the transient zone and the sweet spot (see Figures 7c and 7d), respectively, the corresponding stress drops for these regions are ~7 and ~3 kPa. Such values depend on the relatively unconstrained choices for G and α. However, values twice as large for these constants (i.e., G = 30 GPa and α = 0.6), which are valid for cases where $W \approx L$, would affect the estimated stress drops by a factor of 1.5 to 3, which are still in good agreement with the peak stresses of tens of kPa dynamically induced by the surface waves of the 2010 Maule earthquake, which triggered a large number of tremors in Guerrero during the 2009–2010 SSE [*Zigone et al.*, 2012]. Spatial variations in the stress drop

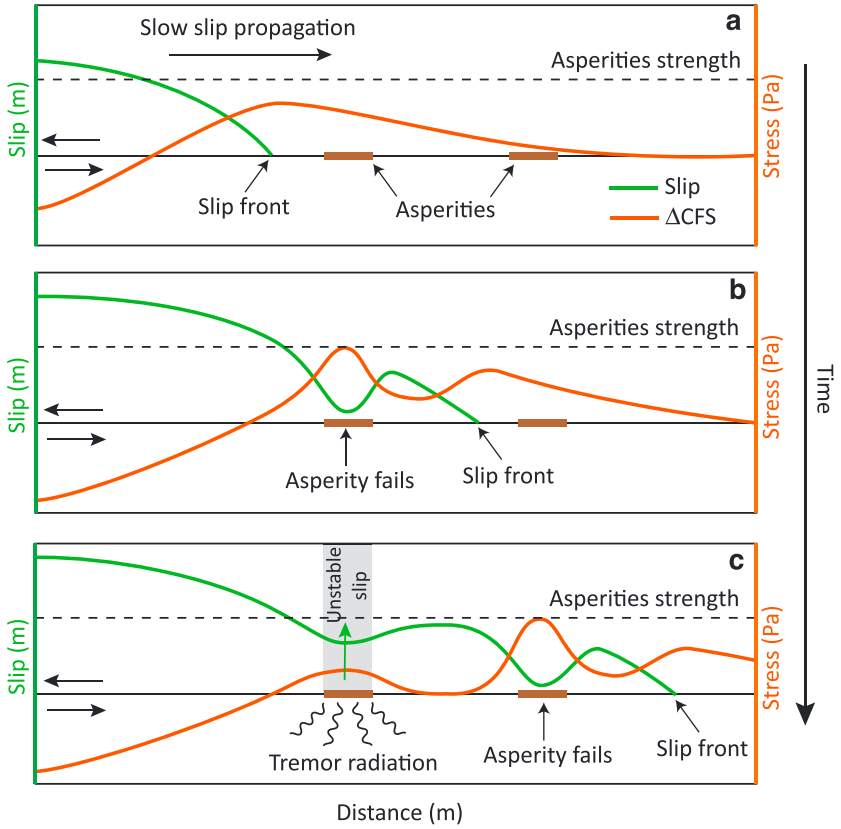

Figure 9. Cartoon illustrating the causal relationship between the SSEs and the TTs as suggested by our analysis. The stress ahead of the slip front does not break tremor asperities. It is the stable slip surrounding the asperities that brings them to failure behind the slip front. See text for more details.

during the SSE suggest that tremor asperities updip in the transient zone can support higher stresses (i.e., around 2.3 times larger) than those downdip in the sweet spot. Such variations, which can be interpreted as changes of the yielding levels in both regions, may be associated either with variations of the asperities' density in the plate interface [*Yabe and Ide*, 2014] or changes in the distribution of sources of fluids, which would translate into variations of pore pressure and thus of the effective stresses along the interface. We point out that the second hypothesis seems more plausible in Guerrero considering that thermal modeling of the subducted Cocos plate predicts mineralogical phase transformations in the slab releasing large amounts of fluids right in the sweet spot [*Manea and Manea*, 2011].

Our results imply that the ΔCFS induced around the SSE slipping regions might not be enough to break the tremor asperities. Typical values of ΔCFS in the sweet spot during the main phase of the SSE are of the order of few kPa (e.g., up to 2.5 kPa in Figure 4b), which are clearly not large enough to trigger tremor as suggested by Figure 5b, where no overall correlation is found between the TT activity and the regions with positive values of ΔCFS. However, during the late phase of the 2006 SSE (i.e., the last 3 months), this is not true, as revealed by the higher consistency between the TT activity and ΔCFS than with the slip (Figure 3). One possible explanation for the low consistency with slip in that period is that tremor bursts in September and November (see black line in Figure 3) correspond to reactivated slip transients not resolved in the SSE inversion by *Radiguet et al.* [2012]. Another possibility is that stronger tremor asperities were loaded during the passage of the SSE front and then broken by trailing increments of the CFS, as suggested by the last snapshot of the right column in Figure 2. Our findings then suggest that the causal relationship between SSEs and TTs primarily depends on the stressing rate history of tremor asperities, which, in turn, is modulated by the slip rate surrounding the asperities. Figure 9 illustrates this idea. Once the SSE approaches the TT source region, it induces an increase of the shear stress (or ΔCFS) ahead of the slip front (Figure 9a). At this point, the stress concentration does not exceed the strength level of the

asperities. As soon as the slip front reaches the tremor region, the slip rate surrounding the locked asperities keeps stressing them till they break (Figure 9b), increasing thus the TT occurrence rate behind the slip front (Figure 9c). This mechanism has also been suggested to explain the tremor genesis in Cascadia [*Wech and Bartlow*, 2014]. As discussed before, the strength of the asperities in the sweet spot is significantly lower (about 2.3 times lower) than in the transient zone, which makes the former region much more sensitive to tiny stress perturbations due to small dislocations associated with short-term SSEs that we have shown take place in the sweet spot.

TTs and LFEs are sensitive to small stress perturbations induced by tides in different subduction zones. Recent studies found that the tremor rate and the tidal stress changes obey an exponential relationship [*Thomas et al*., 2012; *Beeler et al*., 2013; *Houston*, 2015; *Yabe et al*., 2015]. *Houston* [2015] observed that tremor rate during the late stage of the ETS is an exponential function of the ΔCFS. Since our results point out that the ΔCFS is not linearly related with the occurrence rate of TTs and LFEs, i.e., they have very low correlation coefficients (top panels of Figures 4 and 5b), we explored the possibility that changes in the rate of these events follow an exponential function of the ΔCFS induced by the SSEs. We performed several tests in different TT regions where we computed the ΔCFS using different values of the friction and Skempton coefficients and compared with the associated tremor rates. However, we did not find a convincing exponential trend as observed for tidal stresses.

The spatial-temporal correlation between tremor activity and the slip rate during the 2006 long-term SSE is clear from our results. However, other SSEs should be analyzed to generalize our conclusions. We performed the same analysis for the 2009–2010 SSE in Guerrero using the slip rate imaging determined by *Radiguet et al*. [2012]. During such event, the MASE array was not longer in operation so we generated a TT catalog using five to seven broadband stations deployed in Guerrero during the G-Gap project. However, the sparsity of the array and the limited time span of the data, which did not cover the complete duration of the SSE, prevented us from obtaining exhaustive TT locations to generate consistent correlation maps such as those of Figure 5.

8. Conclusions

High-resolution tremor locations obtained with the TREP method allowed us to make a detailed analysis of the occurrence rate of TTs during the long-term 2006 SSE. Results from the analysis revealed a consistently high spatial-temporal correlation between the SSE slip rate and the occurrence rate of TT along both the transient zone (updip) and the sweet spot (downdip). The absence of correlation with the SSE-induced ΔCFS leads us to discard the hypothesis advanced by previous authors that the stress transferred from the updip slipping regions acts as the main mechanism triggering tremor downdip in the sweet spot. Our quantitative results suggest that the SSE slip rate is the main parameter modulating the TT activity in the whole Guerrero region. This conjecture implies that the causal relationship between SSEs and the TT activity directly depends on the stressing rate history of the tremor asperities, which, in turn, is modulated by the slip rate in the surrounding regions (Figure 9). Such conclusion supports the idea that TT can be used as a monitoring tool to infer the occurrence of slow slip on the plate interface [e.g., *Wech et al*., 2009; *Frank et al*., 2015b; *Frank*, 2016]. However, care should be taken with the long-term SSEs in Guerrero because the location of the maximum slip does not coincide with the regions of maximum TT activity. A clear example of this is that despite tremor activity dominates in the sweet spot, where we found the highest correlation coefficients with the slip rate, the amount of slip there (3 to 7 cm, Figure 1) is about 3 times smaller than updip in the transient zone. We have estimated that the strength of the asperities radiating tremor in the sweet spot is around ~3.2 kPa, which is ~2.3 times smaller than the corresponding value updip in the transient zone and which makes the former region more sensitive to tiny stress perturbations such as those induced by teleseismic surface waves and short-term SSEs. In addition, we used the LFE rate history during the 2006 SSE and interlong-term SSE periods to constrain the slip distribution of the short-term SSEs in Guerrero. Our results show that these events take place further downdip (about 35 km) than previously estimated by *Frank et al*. [2015b] (Figure 7a) with maximum slip of about 8 mm in the sweet spot (Figure 8). This new model features a continuum of slow-slip regions covering the entire tremor zone. Although further analysis of different SSEs is still necessary to confirm that the slip rate is the parameter that systematically controls the tremor rate in the region, this study provides the first quantitative insights into the causal relationship between TTs and SSEs in Guerrero, Mexico.

Acknowledgments
Seismic data set from the Meso-America Subduction Experiment is available at web.gps.caltech.edu/~clay/MASEdir/data_avail.html. Tectonic tremor catalog is available upon request to the corresponding author. We thank William Frank for sharing his LFE catalog and counts. We also thank Vladimir Kostoglodov and Allen Husker for fruitful discussions and suggestions and both reviewers' comments that helped us to substantially improve the manuscript. This work was supported by the UNAM-PAPIIT grants IN113814 and IN110514, the Japan-Mexico SATREPS project funded by JST/JICA/UNAM/CONACyT, and the graduate school scholarships by the Consejo Nacional de Ciencia y Tecnología (CONACyT).

References

Audet, P., M. G. Bostock, N. I. Christensen, and S. M. Peacock (2009), Seismic evidence for overpressured subducted oceanic crust and megathrust fault sealing, *Nature*, *457*, 76–78, doi:10.1038/nature07650.

Bartlow, N. M., N. M. Bartlow, S. Miyazaki, S. Miyazaki, A. M. Bradley, A. M. Bradley, P. Segall, and P. Segall (2011), Space-time correlation of slip and tremor during the 2009 Cascadia slow slip event, *Geophys. Res. Lett.*, *38*, L18309, doi:10.1029/2011GL048714.

Bartlow, N. M., L. M. Wallace, R. J. Beavan, S. Bannister, and P. Segall (2014), Time-dependent modeling of slow slip events and associated seismicity and tremor at the Hikurangi subduction zone, New Zealand, *J. Geophys. Res. Solid Earth*, *119*, 734–753, doi:10.1002/2013JB010609.

Beeler, N. M., A. Thomas, R. Bürgmann, and D. Shelly (2013), Inferring fault rheology from low-frequency earthquakes on the San Andreas, *J. Geophys. Res. Solid Earth*, *118*, 5976–5990, doi:10.1002/2013JB010118.

Beroza, G. C., and S. Ide (2011), Slow earthquakes and nonvolcanic tremor, *Annu. Rev. Earth Planet. Sci.*, *39*(271), 296, doi:10.1146/annurev-earth-040809-152531.

Caltech (2007), Meso-America Subduction Experiment (MASE) dataset, doi:10.7909/C3RN35SP.

Campillo, M., S. K. Singh, N. Shapiro, J. Pacheco, and R. B. Herrmann (1996), Crustal structure south of the Mexican volcanic belt, based on group velocity dispersion, *Geofis. Int.*, *35*, 361–370.

Cotte, N., A. Walpersdorf, V. Kostoglodov, M. Vergnolle, J.-A. Santiago, I. Manighetti, and M. Campillo (2009), Anticipating the next large silent earthquake in Mexico, *Eos. Trans. AGU*, *90*(21), 181–182, doi:10.1029/2009EO210002.

Cruz-Atienza, V. M., A. Husker, D. Legrand, E. Caballero, and V. Kostoglodov (2015), Nonvolcanic tremor locations and mechanisms in Guerrero, Mexico, from energy-based and particle motion polarization analysis, *J. Geophys. Res. Solid Earth*, *120*, 275–289, doi:10.1002/2014JB011389.

Frank, W. B. (2016), Slow slip hidden in the noise: The intermittence of tectonic release, *Geophys. Res. Lett.*, *43*, 10,125–10,133, doi:10.1002/2016GL069537.

Frank, W. B., N. M. Shapiro, V. Kostoglodov, A. L. Husker, M. Campillo, J. S. Payero, and G. A. Prieto (2013), Low-frequency earthquakes in the Mexican sweet spot, *Geophys. Res. Lett.*, *40*, 2661–2666, doi:10.1002/grl.50561.

Frank, W. B., N. M. Shapiro, A. L. Husker, V. Kostoglodov, A. Romanenko, and M. Campillo (2014), Using systematically characterized low-frequency earthquakes as a fault probe in Guerrero, Mexico, *J. Geophys. Res. Solid Earth*, *119*, 7686–7700, doi:10.1002/2014JB011457.

Frank, W. B., N. M. Shapiro, A. L. Husker, V. Kostoglodov, H. S. Bhat, and M. Campillo (2015a), Along-fault pore-pressure evolution during a slow-slip event in Guerrero, Mexico, *Earth Planet. Sci. Lett.*, *413*, 135–143, doi:10.1016/j.epsl.2014.12.051.

Frank, W. B., M. Radiguet, B. Rousset, N. M. Shapiro, A. L. Husker, V. Kostoglodov, N. Cotte, and M. Campillo (2015b), Uncovering the geodetic signature of silent slip through repeating earthquakes, *Geophys. Res. Lett.*, *42*, 2774–2779, doi:10.1002/2015GL063685.

García, D., S. K. Singh, M. Herraíz, J. F. Pacheco, and M. Ordaz (2004), Inslab earthquakes of central Mexico: Q, source spectra and stress drop, *Bull. Seismol. Soc. Am.*, *94*, 789–802.

Hawthorne, J. C., M. G. Bostock, A. A. Royer, and A. M. Thomas (2016), Variations in slow slip moment rate associated with rapid tremor reversals in Cascadia, *Geochem. Geophys. Geosyst.*, *17*, 4899–4919, doi:10.1002/2016GC006489.

Hirose, H., and K. Obara (2010), Recurrence behavior of short-term slow slip and correlated nonvolcanic tremor episodes in western Shikoku, southwest Japan, *J. Geophys. Res.*, *115*, B00A21, doi:10.1029/2008JB006050.

Hirose, H., Y. Asano, K. Obara, T. Kimura, T. Matsuzawa, S. Tanaka, and T. Maeda (2010), Slow earthquakes linked along dip in the Nankai subduction zone, *Science*, *330*, 1502, doi:10.1126/science.1197102.

Houston, H. (2015), Low friction and fault weakening revealed by rising sensitivity of tremor to tidal stress, *Nat. Geosci.*, *8*(5), 409–415, doi:10.1038/ngeo2419.

Husker, A., S. Peyrat, N. Shapiro, and V. Kostoglodov (2010), Automatic non-volcanic tremor detection in the Mexican subduction zone, *Geofis. Int.*, *49*(1), 17–25.

Husker, A. L., V. Kostoglodov, V. M. Cruz-Atienza, D. Legrand, N. M. Shapiro, J. S. Payero, M. Campillo, and E. Huesca-Pérez (2012), Temporal variations of non-volcanic tremor (NVT) locations in the Mexican subduction zone: Finding the NVT sweet spot, *Geochem. Geophys. Geosyst.*, *13*, Q03011, doi:10.1029/2011GC003916.

Ida, Y. (1973), The maximum acceleration of seismic ground motion, *Bull. Seismol. Soc. Am.*, *63*(3), 959–968.

Ide, S., D. R. Shelly, and G. C. Beroza (2007), Mechanism of deep low frequency earthquakes: Further evidence that deep non-volcanic tremor is generated by shear slip on the plate interface, *Geophys. Res. Lett.*, *34*, L03308, doi:10.1029/2006GL028890.

Iglesias, A., R. W. Clayton, X. Pérez-Campos, S. K. Singh, J. F. Pacheco, D. García, and C. Valdés-González (2010), S wave velocity structure below central Mexico using high-resolution surface wave tomography, *J. Geophys. Res.*, *115*, B06307, doi:10.1029/2009JB006332.

Kim, Y., R. W. Clayton, and J. M. Jackson (2010), Geometry and seismic properties of the subducting Cocos plate in central Mexico, *J. Geophys. Res.*, *115*, B06310, doi:10.1029/2009JB006942.

Kostoglodov, V., S. K. Singh, J. A. Santiago, S. I. Franco-Sanchez, K. M. Larson, A. R. Lowry, and R. G. Bilham (2003), A large silent earthquake in the Guerrero seismic gap, Mexico, *Geophys. Res. Lett.*, *30*(15), 1807, doi:10.1029/2003GL017219.

Kostoglodov, V., A. L. Husker, N. M. Shapiro, J. S. Payero, M. Campillo, N. Cotte, and R. W. Clayton (2010), The 2006 slow slip event and nonvolcanic tremor in the Mexican subduction zone, *Geophys. Res. Lett.*, *37*, L24301, doi:10.1029/2010GL045424.

Manea, V. C., and M. Manea (2011), Flat-slab thermal structure and evolution beneath Central Mexico, *Pure Appl. Geophys.*, *168*(8–9), 1475–1487, doi:10.1007/s00024-010-0207-9.

Maury, J., S. Ide, V. M. Cruz-Atienza, V. Kostoglodov, G. González-Molina, and X. Pérez-Campos (2016), Comparative study of tectonic tremor locations: Characterization of slow earthquakes in Guerrero, Mexico, *J. Geophys. Res. Solid Earth*, *121*, 5136–5151, doi:10.1002/2016JB013027.

Obara, K. (2002), Nonvolcanic deep tremor associated with subduction in southwest Japan, *Science*, *296*(5573), 1679–1681.

Obara, K. (2011), Characteristics and interactions between non-volcanic tremor and related slow earthquakes in the Nankai subduction zone, southwest Japan, *J. Geodyn.*, *52*(3–4), 229–248, doi:10.1016/j.jog.2011.04.002.

Obara, K., and H. Hirose (2006), Non-volcanic deep low-frequency tremors accompanying slow slips in the southwest Japan subduction zone, *Tectonophysics*, *417*, 33–51, doi:10.1016/j.tecto2005.04013.

Olsen, K. B., et al. (2009), ShakeOut-D: Ground motion estimates using an ensemble of large earthquakes on the southern San Andreas fault with spontaneous rupture propagation, *Geophys. Res. Lett.*, *36*, L04303, doi:10.1029/2008GL036832.

Payero, J. S., V. Kostoglodov, N. Shapiro, T. Mikumo, A. Iglesias, X. Pérez-Campos, and R. W. Clayton (2008), Nonvolcanic tremor observed in the Mexican subduction zone, *Geophys. Res. Lett.*, *35*, L07305, doi:10.1029/2007GL032877.

Peacock, S. M., N. I. Christensen, M. G. Bostock, and P. Audet (2011), High pore pressures and porosity at 35 km depth in the Cascadia subduction zone, *Geology*, *39*(5), 471–474, doi:10.1130/G31649.1.

Peng, Z., and J. S. Gomberg (2010), An integrated perspective of the continuum between earthquakes and slow-slip phenomena, *Nat. Geosci.*, *3*, 599–607, doi:10.1038/ngeo940.

Pérez-Campos, X., Y. Kim, A. L. Husker, P. M. Davis, R. W. Clayton, A. Iglesias, J. F. Pacheco, S. K. Singh, V. C. Manea, and M. Gurnis (2008), Horizontal subduction and truncation of the Cocos plate beneath central Mexico, *Geophys. Res. Lett.*, *35*, L18303, doi:10.1029/2008GL035127.

Perry, M., G. A. Spinelli, I. Wada, and J. He (2016), Modeled temperatures and fluid source distributions for the Mexican subduction zone: Effects of hydrothermal circulation and implications for plate boundary seismic processes, *Geochem. Geophys. Geosyst.*, *17*, 550–570, doi:10.1002/2015GC006148.

Radiguet, M., F. Cotton, M. Vergnolle, M. Campillo, B. Valette, V. Kostoglodov, and N. Cotte (2011), Spatial and temporal evolution of a long term slow slip event: The 2006 Guerrero slow slip event, *Geophys. J. Int.*, *184*(2), 816–828, doi:10.1111/j.1365-246X.2010.04866.x.

Radiguet, M., F. Cotton, M. Vergnolle, M. Campillo, A. Walpersdorf, N. Cotte, and V. Kostoglodov (2012), Slow slip events and strain accumulation in the Guerrero gap, Mexico, *J. Geophys. Res.*, *117*, B04305, doi:10.1029/2011JB008801.

Rivet, D., M. Campillo, N. M. Shapiro, V. Cruz-Atienza, M. Radiguet, N. Cotte, and V. Kostoglodov (2011), Seismic evidence of nonlinear crustal deformation during a large slow slip event in Mexico, *Geophys. Res. Lett.*, *38*, L08308, doi:10.1029/2011GL047151.

Rivet, D., et al. (2013), Seismic velocity changes, strain rate and non-volcanic tremors during the 2009–2010 slow slip event in Guerrero, Mexico, *Geophys. J. Int.*, *196*, 447–460, doi:10.1093/gji/ggt374.

Rogers, G., and H. Dragert (2003), Episodic tremor and slip on the Cascadia subduction zone: The chatter of silent slip, *Science*, *300*, 1942–1943, doi:10.1126/science.1084783.

Royer, A. A., A. M. Thomas, and M. G. Bostock (2015), Tidal modulation and triggering of low frequency earthquakes in northern Cascadia, *J. Geophys. Res. Solid Earth*, *120*, 384–405, doi:10.1002/2014JB011430.

Rubin, A. M. (2011), Designer friction laws for bimodal slow slip propagation speeds, *Geochem. Geophys. Geosyst.*, *12*, Q04007, doi:10.1029/2010GC003386.

Rubin, A. M., and J.-P. Ampuero (2009), Self-similar slip pulses during rate-and-state earthquake nucleation, *J. Geophys. Res.*, *114*, B11305, doi:10.1029/2009JB006529.

Rubin, A. M., and J. G. Armbruster (2013), Imaging slow slip fronts in Cascadia with high precision cross-station tremor locations, *Geochem. Geophys. Geosyst.*, *14*, 5371–5392, doi:10.1002/2013GC005031.

Shelly, D. R., G. C. Beroza, and S. Ide (2007), Non-volcanic tremor and low-frequency earthquake swarms, *Nature*, *446*, 305–307, doi:10.1038/nature05666.

Shibazaki, B., and T. Shimamoto (2007), Modelling of short-interval silent slip events in deeper subduction interfaces considering the frictional properties at the unstable-stable transition regime, *Geophys. J. Int.*, *171*, 191–205, doi:10.1111/j.1365-246X.2007.03434.x.

Song, T.-R. A., D. V. Helmberger, M. R. Brudzinski, R. W. Clayton, P. M. Davis, X. Pérez-Campos, and S. K. Singh (2009), Subducting slab ultra-slow velocity layer coincident with silent earthquakes in southern Mexico, *Science*, *324*, 502–506, doi:10.1126/science.1167595.

Schwartz, S. Y., and J. M. Rokosky (2007), Slow-slip events and seismic tremor at circum-Pacific subduction zones, *Rev. Geophys.*, *45*, RG3004, doi:10.1029/2006RG000208.

Thomas, A. M., R. M. Nadeau, and R. Bürgmann (2009), Tremor-tide correlations and near lithostatic pore pressure on the deep San Andreas fault, *Nature*, *462*, 1048–1051, doi:10.1038/nature08654.

Thomas, A. M., R. Bürgmann, D. R. Shelly, N. M. Beeler, and M. L. Rudolph (2012), Tidal triggering of low frequency earthquakes near Parkfield, California: Implications for fault mechanics within the brittle-ductile transition, *J. Geophys. Res.*, *117*, B05301, doi:10.1029/2011JB009036.

Vergnolle, M., A. Walpersdorf, V. Kostoglodov, P. Tregoning, J. A. Santiago, N. Cotte, and S. I. Franco-Sanchez (2010), Slow slip events in Mexico revised from the processing of 11 year GPS observations, *J. Geophys. Res.*, *115*, B08403, doi:10.1029/2009JB006852.

Villafuerte, C. (2016), Evolución de la presión de poro debido a sismos silenciosos. Implicaciones en la generación de tremores tectónicos en Guerrero, México, Master Thesis, 110 pp., Universidad Nacional Autónoma de México, Mexico.

Wech, A. G., K. C. Creager, and T. I. Melbourne (2009), Seismic and geodetic constraints on Cascadia slow slip, *J. Geophys. Res.*, *114*, B10316, doi:10.1029/2008JB006090.

Wech, A. G., and N. M. Bartlow (2014), Slip rate and tremor genesis in Cascadia, *Geophys. Res. Lett.*, *41*, 392–398, doi:10.1002/2013GL058607.

Yabe, S., and S. Ide (2014), Spatial distribution of seismic energy rate of tectonic tremors in subduction zones, *J. Geophys. Res. Solid Earth*, *119*, 8171–8185, doi:10.1002/2014JB011383.

Yabe, S., Y. Tanaka, H. Houston, and S. Ide (2015), Tidal sensitivity of tectonic tremors in Nankai and Cascadia subduction zones, *J. Geophys. Res. Solid Earth*, *120*, 7587–7605, doi:10.1002/2015JB012250.

Zigone, D., D. Rivet, M. Radiguet, M. Campillo, C. Voisin, N. Cotte, A. Walpersdorf, N. M. Shapiro, G. Cougoulat, and P. Roux (2012), Triggering of tremors and slow slip event in Guerrero, Mexico, by the 2010 M_w 8.8 Maule, Chile, earthquake, *J. Geophys. Res.*, *117*, B09304, doi:10.1029/2012JB009160.